

Two new ROSAT discovered high field polars: RX J2022.6–3954 in Sagittarius and RX J0132.7–6554 in Hydrus*

V. Burwitz¹, K. Reinsch¹, K. Beuermann^{1,2}, and H.-C. Thomas⁴

¹ Universitäts-Sternwarte Göttingen, Geismarlandstr. 11, D-37083 Göttingen, Germany

² MPI für Extraterrestrische Physik, Giessenbachstr. 1, D-85740 Garching, Germany

³ MPI für Astrophysik, Karl-Schwarzschild-Str. 1, D-85740 Garching, Germany

Received 21 April 1997 / Accepted 16 June 1997

Abstract. We report the discovery of two new AM Herculis systems (polars), identified as the optical $V \sim 19$ mag and $V \sim 20$ mag counterparts of the soft X-ray sources RX J2022.6–3954 and RX J0132.7–6554 detected during the ROSAT All-Sky Survey and present the results of our optical and X-ray follow-up observations. From the cyclotron emission lines detected in the optical spectra we determine magnetic field strengths in the accretion region of $B = 67(2)$ MG for RX J2022.6–3954 and $B = 68(2)$ MG for RX J0132.7–6554. With $P_{orb} = 78.0176(4)$ min for RX J2022.6–3954 and $P_{orb} = 77.831(8)$ min for RX J0132.7–6554 both objects have orbital periods which lie at the lower limit of the period distribution of CVs. RX J0132.7–6554 is the shortest period polar yet detected. Both objects show no eclipse by the secondary stars, and, therefore must have orbital inclinations of $i \lesssim 85^\circ$. As RX J2022.6–3954 shows a dip due to the accretion stream crossing our line-of-sight and the accretion region on the white dwarf is partially self-eclipsed we can further constrain the orbital inclination and co-latitude of the magnetic pole to be $45^\circ < i < 85^\circ$ and $45^\circ > \delta > 5^\circ$. From the absence of M-star features in the faint phase spectra of both objects we obtain a lower limit for the distance to RX J2022.6–3954 of $d > 190$ pc and to RX J0132.7–6554 of $d > 300$ pc. The high magnetic fields and short orbital periods make both objects highly interesting in the context of the evolution of accreting close-binary systems.

Key words: accretion, accretion disks – stars: individual (RX J2022.6–3954) – stars: individual (RX J0132.7–6554) – stars: novae, cataclysmic variables – stars: magnetic X-rays: stars

Send offprint requests to: burwitz@uni-sw.gwdg.de

* Based on observations collected at the European Southern Observatory, La Silla, Chile with the 2.2-m telescope of the Max-Planck-Society in MPI time and with various telescopes in ESO time (ESO Nos 48.6-002, 51.7-045, 55.D-0383).

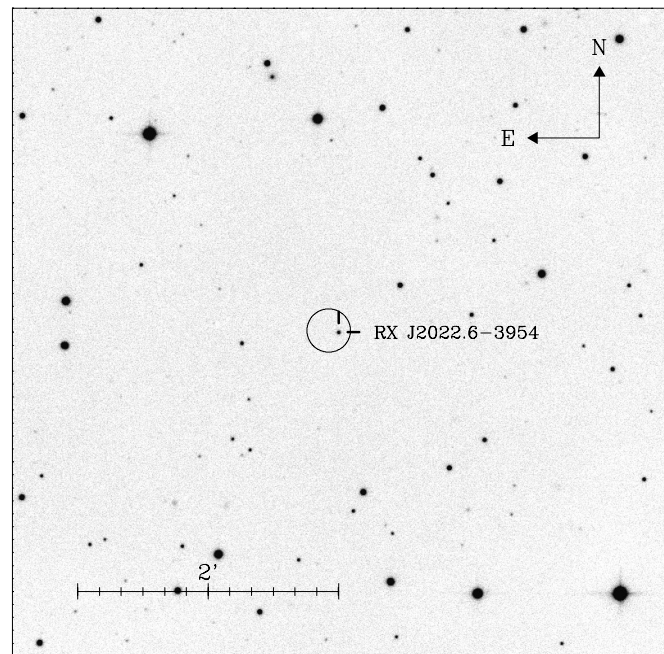


Fig. 1. V-filter CCD image centered on $\alpha_{2000}=20^{\text{h}}22^{\text{m}}37.5$, $\delta_{2000}=-39^{\circ}54'13''$, the position of the $V \sim 19$ mag optical counterpart of the RASS X-ray source RX J2022.6–3954. The uncertainty of the X-ray position is given by the 95% confidence ($\sim 6''$) error circle.

1. Introduction

AM Herculis binaries (polars) have a strong and highly variable soft X-ray flux and can, therefore, easily be selected from the bulk of the sources detected in the ROSAT All-Sky Survey (RASS). Our optical identification of bright, soft, high galactic latitude RASS sources led to the discovery of several new polars providing a significantly improved basis for the study of accretion phenomena in close-binary systems containing white dwarfs with strong magnetic fields, i.e. 7–230 MG (Beuermann & Burwitz 1995, Beuermann et al. 1995, Schwöpe 1995, Warner 1995, Beuermann 1997, and references therein).

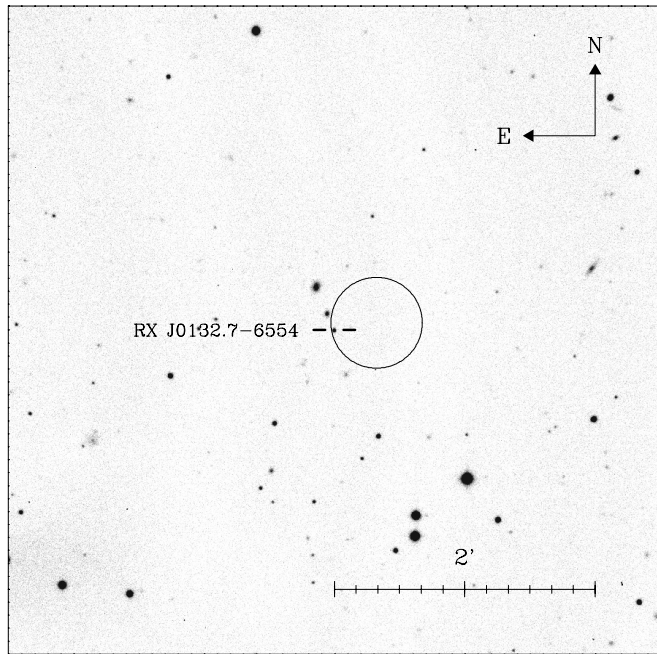


Fig. 2. White-light CCD image centered on $\alpha_{2000}=1^{\text{h}}32^{\text{m}}42^{\text{s}}.0$, $\delta_{2000}=-65^{\circ}54'32''$, the position of the V \sim 20 mag optical counterpart of the RASS X-ray source RX J0132.7–6554. The uncertainty of the X-ray position is given by the 95% confidence ($\sim 13''$) error circle.

In this paper we report the discovery of further two AM Herculis systems, RX J2022.6–3954 and RX J0132.7–6554 (henceforth 2022–39 and 0132–65) which we have identified with the respective V \sim 19 and V \sim 20 mag optical counterparts (see Figs. 1 and 2). Here, we present the analysis of our X-ray data (ROSAT survey and pointed observations) and optical follow-up data (CCD photometry and time resolved spectroscopy) and discuss the importance of these short-period, high-field, close-binary systems in the context of the evolution of magnetic CVs.

2. Observations

2.1. Optical observations

Our optical identification spectra and time-resolved follow-up observations were collected during five observing runs at the European Southern Observatory (ESO) at La Silla, Chile. Low-resolution spectroscopy was obtained with EFOSC2 and CCD#19 at the ESO/MPI 2.2-m telescope in July and November 1995 and with EFOSC1 and CCD#26 at the 3.6-m telescope in January 1992 (discovery spectrum of 0132–65). Slit widths of $1''.0$, $1''.5$ and $2''.0$ were used to adjust to the different seeing conditions during the individual nights. CCD photometry was performed with CCD#29 at the Dutch 0.9-m telescope in September 1993, with CCD#28 at the Danish 1.54-m telescope in July 1995, and with CCD#19 at the 2.2-m telescope in November 1995. The details of the observations are given

Table 1. Journal of optical observations of 2022–39 and 0132–65.

Date	HJD range (+2400000)	No. Exp.	Wavelength range (Å)	Res. (Å)	Exp. (s)
<i>RX J2022.6–3954 :</i>					
CCD photometry					
95/07/08	49906.6582–.7725	51	V		120
95/11/14	50035.5066–.6326	156	V		30/20
95/11/15	50036.5055–.6113	141	V		30/20
95/11/24	50045.5082–.5551	61	V		20
Optical spectroscopy					
95/07/02	49901.7440–.7556	2	3500–9120	48	600
95/07/03	49902.6919–.8148	14	3500–9120	36	480
95/07/04	49903.7355–.8611	1/8	3500–9120	48	600/900
95/11/11	50032.5187–.5863	18	3800–9120	24	300
<i>RX J0132.7–6554 :</i>					
CCD photometry					
93/09/18	49248.5539–.7758	77	WL		180
93/09/19	49249.5454–.7175	67	WL		180
95/11/16	50037.5155–.6232	81	WL		60
95/11/16	50037.8058–.8572	39	WL		60
95/11/17	50038.6683–.7766	81	WL		60
95/11/26	50099.6061–.6867	61	WL		60
Optical spectroscopy					
92/01/02	48624.6088	1	3716–6790	15	1800
95/07/02	49901.7820	1	3800–9120	48	720
95/07/02	49901.7955	1	3800–9120	48	720
95/11/26	50048.6429	1	3800–9120	48	720
95/11/26	50048.6484	1	3800–9120	48	2400
95/11/26	50048.6894	1	3800–9120	48	1800

in Table 1. All observations except the July 1995 spectroscopy were done under photometric conditions.

CCD#19 is a front illuminated 1024×1024 pixel² Thompson CCD with $19 \times 19 \mu\text{m}^2$ pixels, CCD#26 and CCD#29 are back illuminated thin 512×512 pixel² Tektronics CCDs with $27 \times 27 \mu\text{m}^2$ pixels, and CCD#28 is a back illuminated thin 1024×1024 pixel² Tektronics CCD with $24 \times 24 \mu\text{m}^2$ pixels.

The long-slit spectroscopic CCD images were reduced using the MIDAS software packages provided by ESO. A flux calibration was obtained from observations of spectrophotometric standard stars (Hamuy et al. 1992, 1994).

From the CCD direct images, differential photometry was derived by integrating the fluxes of the object, nearby comparison stars contained in the field of view, and the sky background using circular apertures. An absolute calibration of the V-filter data was derived from observations of photometric standard stars (Landolt 1992). The stability of the photometry was checked from the flux differences of the comparison stars. For the comparison stars of 2022–39 flux variations of ~ 0.006 mag and ~ 0.008 mag were found for the July 1995 and November 1995 data, respectively. For those of 0132–65 somewhat larger variations of ~ 0.04 mag and ~ 0.03 mag were determined for the September 1993 and November 1995 data, respectively, as

Table 2. Journal of ROSAT X-ray observations of 2022–39 and 0132–65.

Date	HJD range (+2400000)	Detector	# of OBIs ^a	Count rate (cts/s)	HR1	Exp. (s)
<i>RX J2022.6–3954 :</i>						
90/10/07	48171.6450–	PSPC	21	0.35(5)	–0.84(5)	474
90/10/15	48179.9478	(RASS)				
<i>RX J0132.7–6554 :</i>						
90/11/09	48204.7947–	PSPC	16	0.30(9)	–0.93(4)	341
90/11/17	48212.9347	(RASS)				
93/11/03–	49295.0015–	PSPC	5	0.044(3)	–1.0(1)	5144
93/11/15	49306.8921					
94/06/01–	49505.3782–	PSPC	2	0.047(1)	–0.81(15)	1912
94/06/05	49509.3058					
95/05/17–	49855.1313–	HRI	8	0.0011(3)		9629
95/06/09	49878.2159					

^a OBI: observation interval**Table 3.** Dip times of 2022–39 and optical maxima times of 0132–65.

Time of dip HJD (HJD–2400000 days)	Error (days)	Time of dip HJD (HJD–2400000 days)	Error (days)
<i>RX J2022.6–3954 : Dip times</i>			
48175.4396	0.0060	50035.6223	0.0008
49906.6775	0.0015	50036.5443	0.0008
49906.7307	0.0015	50036.5978	0.0008
50035.5142	0.0008	50045.5381	0.0008
50035.5681	0.0008		
<i>RX J0132.7–6554 : Times of maxima</i>			
49248.5793	0.0015	50037.5557	0.0015
49248.6346	0.0015	50037.6100	0.0015
49248.6900	0.0015	50037.8235	0.0015
49248.7453	0.0015	50038.6901	0.0015
49249.5545	0.0015	50038.7438	0.0015
49249.6071	0.0015	50047.6074	0.0015
49249.6629	0.0015	50047.6628	0.0015

weaker comparison stars had to be used. The V-magnitude for 0132–65 was derived from our spectrophotometry.

2.2. X-ray observations

In addition to the RASS observations of 2022–39 and 0132–65 pointed PSPC and HRI observations of 0132–65 were obtained with ROSAT. The details of the X-ray observations (such as observing dates, exposure times, number of observation intervals, mean count rates and hardness ratios) are summarized in Table 2. The hardness ratio HR1 denotes the number of photons above 0.4 keV minus the number of photons below 0.4 keV divided by the total number of photons in the 0.1–2.4 keV ROSAT energy band. All the X-ray data were reduced using the EXSAS software package provided by the MPE Garching (Zimmermann et al. 1993).

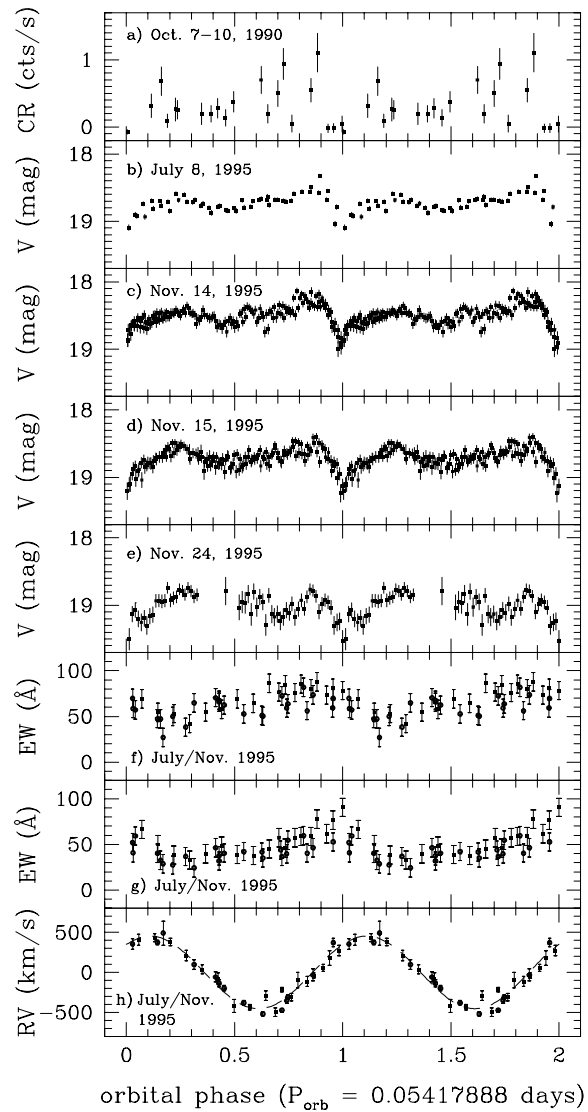


Fig. 3a–h. X-ray and optical modulations of 2022–39. The data in all panels are folded using the ephemeris given in equation (1). **a** RASS X-ray lightcurve, **b–e** optical V-filter lightcurves obtained on July 8, 1995, Nov. 14, 15, and 24, 1995, respectively, **f, g** phase folded equivalent widths of H α and He II λ 4686, respectively, obtained from the July (●) and November (▲) 1995 spectroscopy, **h** average radial velocities of the H α , H β , and He II λ 4686 emission lines measured in July (●) and November (▲) 1995.

3. Results

3.1. RX J2022.6–3954

3.1.1. Orbital period and modulations

The V-filter lightcurves of 2022–39 show pronounced dips of ~ 0.5 mag, recurring about every 78 min which proved to be the orbital period of the system. Our CCD photometry covers two full orbits during one night in July 1995 with a time resolution of ~ 3 min and five additional orbits spread over a baseline of 10 nights in November 1995 (time resolution ~ 40 – 60 sec). From

these data we have obtained eight dip timings (cf. Table 3) which are suitably well spaced that a period search could be done and alias periods could be eliminated. Based on the combined July and November 1995 photometry, a χ^2 -fit to the dip timings yields the following ephemeris for the optical dip:

$$T_{\text{dip}} = \text{HJD } 2450004.84916(24) + 0.05417888(23) \times E \quad (1)$$

The V-filter lightcurves folded on this period are shown for the individual nights in Fig. 3b-e. The average brightness is somewhat variable from night to night ($V \sim 18.4\text{--}19.0$), probably due to fluctuations of the accretion rate. The shape of the lightcurves is roughly constant with maximum flux occurring around orbital phase 0.8 to 0.9. A second although generally lower maximum is observed at phase 0.2–0.3. The full amplitude of the orbital variation is ~ 0.8 mag. The equivalent widths of the $H\alpha$ and $\text{He II } \lambda 4686$ emission lines (Fig. 3f,g) obtained from our July and November 1995 spectroscopy vary by about 50% over the orbit. Maximum equivalent widths are observed around phase 0.9 for $H\alpha$ and around phase 0.0 for He II .

As our low-resolution spectroscopy does not resolve individual components of the Balmer and $\text{He II } \lambda 4686$ emission lines we have determined radial velocities by fitting single Gauss functions to the line profiles. Eventhough the equivalent width variations are different for the Balmer and $\text{He II } \lambda 4686$ emission lines the corresponding radial velocities do not significantly differ. The radial velocities show a strong modulation with the photometric period. The radial velocity amplitude derived from a sinusoidal fit to the average Doppler shifts of $H\alpha$, $H\beta$, and He II is (454 ± 18) km/s (Fig. 3h).

The RASS X-ray data folded over the optical period (Fig. 3a) show a discontinuity of the 0.1–2.4 keV flux during the X-ray bright phase when the flux decreases from ~ 1 cts/s to the detection limit. Our optical ephemeris is sufficiently accurate to determine the orbital phase of the X-ray dip to be 0.92 ± 0.10 . It is not uncommon in AM Herculis systems that X-ray and optical dips coincide in orbital phase as both may be caused by an eclipse of the accretion region on the white dwarf by the accretion stream. If we include the timing of the X-ray dip in our period search, we find an improved dip ephemeris

$$T_{\text{dip}} = \text{HJD } 2450004.84916(13) + 0.054179039(12) \times E \quad (2)$$

3.1.2. Magnetic field strength

The optical spectra of 2022–39 show strong Balmer, He I, and He II emission lines with variable profiles characteristic of AM Herculis binaries. The underlying continuum is flat during the optical dip phase ($\varphi \sim -0.05 - 0.05$) and shows broad humps during the bright phase ($\varphi \sim 0.15 - 0.30$ and $\varphi \sim 0.75 - 0.92$). These humps are more obvious in the difference spectrum between bright and dip phase spectra and are typical for cyclotron emission radiated from an accretion plasma in a strong magnetic field (cf. Fig. 4). We have identified the hump pattern in the difference spectrum with the 2nd, 3rd, and 4th cyclotron harmonics corresponding to a magnetic field strength $B = (67 \pm 2)$ MG.

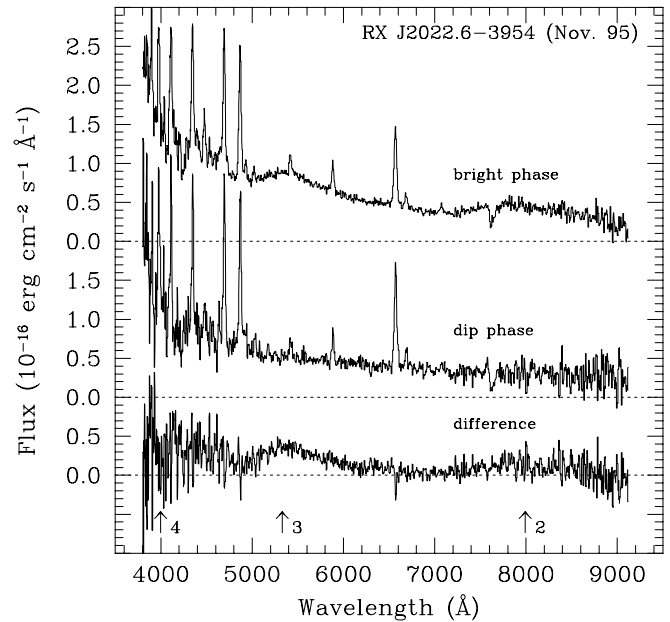


Fig. 4. Low-state bright-phase, dip-phase, and difference spectra of 2022–39 observed in Nov. 1995 (from top to bottom). The positions of the 2nd, 3rd, and 4th cyclotron harmonics expected for a magnetic field strength of 67 MG are marked by arrows.

3.1.3. Distance estimate

In the dip phase optical spectra of 2022–39 no features related to the M dwarf secondary can be seen down to the noise level. This implies that the contribution of the secondary star to the total flux in the R band must be less than about 10%. Therefore, the method described by Bailey (1981) can be adapted to derive a lower limit for the distance of 2022–39. A Roche-lobe filling red dwarf with an orbital period of 1.3 hours is likely to have a radius of $\sim 0.13 R_{\odot}$ and a mass of $\sim 0.1 M_{\odot}$ (depending only weakly on $M_{wd} \sim 0.6 - 1.4 M_{\odot}$). A single M-dwarf with similar mass has a spectral type later than M5 such as VB 8 which has infrared colours $V-K = 7.92$ and $R-K = 5.83$ (Reid & Gilmore 1984). Using the improved surface brightness relationship for M dwarfs (Ramseyer 1994) and $V-K$ of VB 8, we obtain a K surface brightness $S_K = 5.44$ for the secondary in 2022–39. With $R-K$ of VB 8 and $R > 22.1$ from the Nov. 1995 dip phase spectrum of 2022–39, this leads to a lower limit $d > 190$ pc for the distance of 2022–39.

3.2. RX J0132.7–6554

3.2.1. Orbital period and modulations

Due to the low mean brightness ($V \sim 20$ mag) of the system, photometry of 0132–65 was obtained in white light in order to reach sufficient time resolution and signal-to-noise of the data. Time resolutions of ~ 4 min and ~ 1.5 min could be achieved with the 0.9-m and 2.2-m telescopes, respectively. The lightcurves obtained during both runs have similar shapes and modulation amplitudes. The mean amplitudes of the lightcurves are

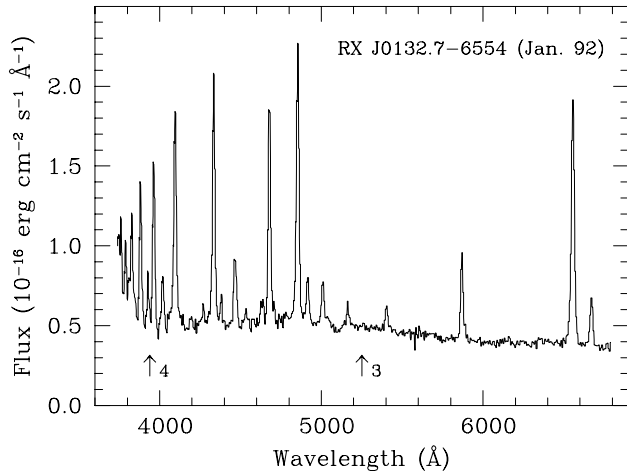


Fig. 5. Identification spectrum of 0132–65 obtained in January 1992 during a high-state. The positions of the 3rd and 4th cyclotron harmonics seen in the low state spectra are marked by arrows.

~ 1 mag. A bright phase with a symmetrical rise and decline lasts about 65% of the time and repeats about every 78 min. During the faint phase the shapes of the lightcurves are flat with some fluctuations. Seven optical maxima have been observed in two subsequent nights in September 1993 and further seven maxima distributed over 10 nights in November 1995 (cf. Table 3). A time series analysis of both data sets yields an optical period $P = 77.831(8)$ min. Unfortunately, the baseline between both observing runs is too long to derive an unambiguous period from the combined data set. The optical lightcurves of the two runs folded on the best period are shown in Fig. 6 together with the ROSAT PSPC data obtained in November 1993. The latter are the only X-ray data of 0132–65 which cover an entire orbit with a sufficient countrate to generate a decent lightcurve. Our optical ephemeris is sufficient to get the phasing between the September 1993 photometry and the November 1993 X-ray data with an accuracy of ~ 0.1 . The maximum of the 0.1–2.4 keV soft X-ray flux occurs during the optically faint phase. As only ~ 10 source counts have been obtained during our ROSAT HRI observation of 0132–65 no light curve could be produced from these data.

3.2.2. Magnetic field strength

The identification spectrum of 0132–65 (cf. Fig. 5) obtained in January 1992 clearly shows the typical optical emission lines (strong Balmer, He I, and He II) found in polars during their high-state. These lines are much weaker in our spectra obtained in July and Nov. 1995 (cf. Fig. 7) which show the system in a low state. In July 1995 only two spectra with exposure times of 12 min each were obtained as the weather was not very collaborative and the system turned out to be too faint to obtain time resolved spectroscopy. Even though the signal-to-noise ratio is not good, the difference of both spectra clearly shows humps in the optical continuum which we have identified as the 2nd, 3rd,

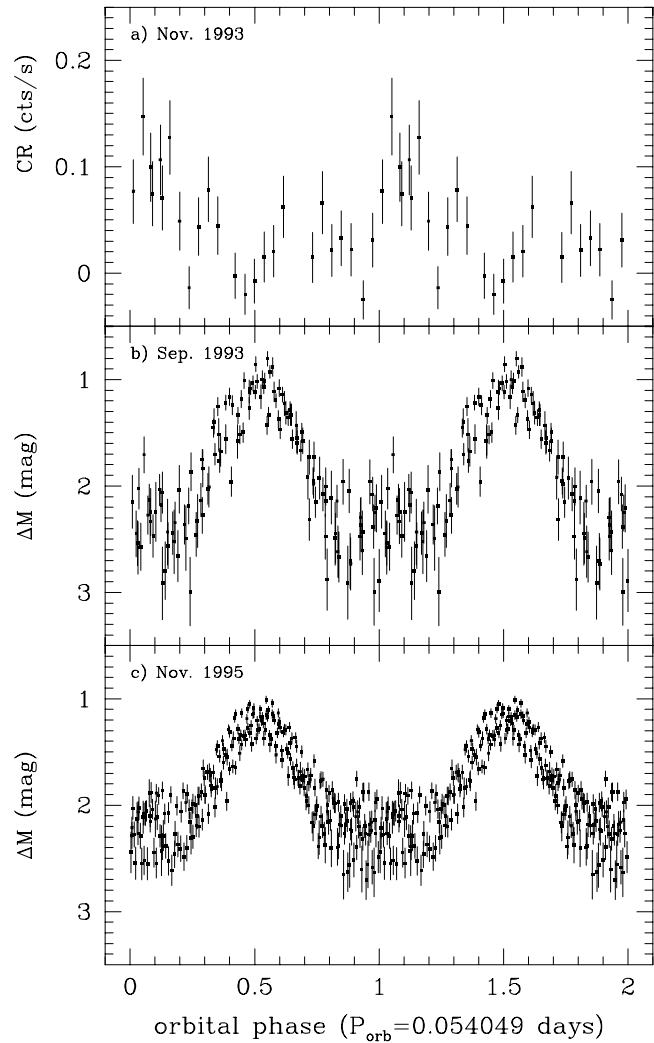


Fig. 6. X-ray and optical variations of 0132–65 folded over its optical period. a) 0.1–2.4 keV lightcurve measured with the ROSAT PSPC in Nov. 1993, b), c) white light CCD photometry obtained in Sep. 1993 and in Nov. 1995, respectively. Arbitrary zeropoints were used for both optical light curves with $\varphi = 0.0$ centered on the optical minimum. For the X-ray lightcurve the same zeropoint has been used as for the Sep. 1993 optical data

and 4th cyclotron harmonics corresponding to a magnetic field strength of (68 ± 2) MG (cf. Fig. 7, bottom). After improving the ephemeris using CCD photometry we obtained two spectra of 0132–65 in November 1995, one 40 min spectrum centered on the bright phase and one 30 min spectrum centered on the faint phase. The difference of these two spectra shows cyclotron humps at the same positions confirming the 68 MG magnetic field strength derived from the July 1995 spectra (cf. Fig. 7).

3.2.3. Distance estimate

Like in 2022–39 no features related to the M dwarf secondary can be seen in the faint phase optical spectra of 0132–65. Therefore, the contribution of the secondary star to the total flux

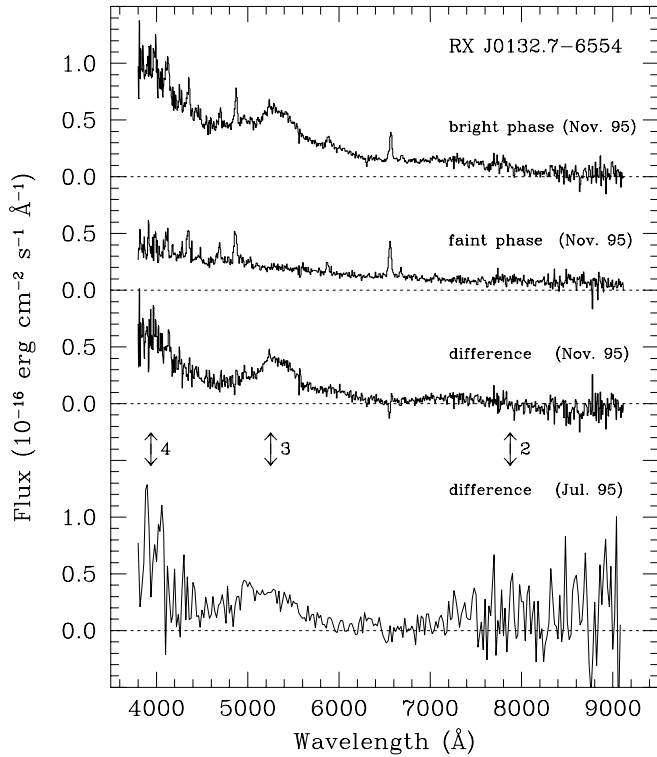


Fig. 7. Low-state bright and faint phase spectra of 0132–65 obtained in Nov. 1995, and difference spectra bright–faint phase for the Nov. and July 1995 data (from top to bottom). The positions of the 2nd, 3rd, and 4th cyclotron harmonics which correspond to a magnetic field strength of 68 MG are shown.

Table 4. Summary of spectral fits to the survey and pointed PSPC data of 2022–39 (fits a-b) and 0132–65 (fits c-e). Parameters given without error range have been fixed for the particular fit. F_{br} and F_{bb} are the unabsorbed fluxes in the 0.1–2.4 keV ROSAT band

N_{H} (10^{19} cm^{-2})	kT_{br} (keV)	kT_{bb} (eV)	F_{br} ($10^{-12} \text{ erg cm}^{-2} \text{ s}^{-1}$)	F_{bb}	χ_r^2	d.o.f.	data set	fit
<i>RX J2022.6–3954</i>								
41.3	20	25	0.015	57.21	0.57	16	Oct.90	(a)
41.3	20	32_{-12}^{+19}	0.010	27.30	0.58	15	Oct.90	(b)
<i>RX J0132.7–6554</i>								
19.0	20	25	0.238	8.08	0.71	12	Nov.90	(c)
$19.0_{-19.0}^{+30.0}$	20	25	0.025	1.56	0.88	18	Nov.93	(d)
19.0	20	25	0.025	1.26	0.94	9	Jun.94	(e)

in R must be less than 10%. Using the same method as described in section 3.1.3 for 2022–39 and $R > 23.1$ from the Nov. 1995 faint phase spectrum of 0132–65 we obtain a lower limit $d > 300$ pc for the distance of 0132–65.

3.3. X-ray spectra

The photon event files of the different datasets of 2022–39 and 0132–65 were binned in such a way that the signal to noise ratio is 2 in each energy bin. Like for other AM Her systems we have fitted two component (blackbody + thermal bremsstrahlung)

models with different parameters to the data. The X-ray spectra are shown in Fig. 8. A summary of the fits we have performed to the data is given in Tab. 4. Due to the low number of photons detected and the poor spectral resolution of the ROSAT PSPC N_{H} and kT_{bb} are poorly constrained for both objects. In order to somewhat restrict the parameters to physically meaningful values we included additional conditions and performed a series of fits to the spectra in which we held several parameters fixed. In all our fits we assumed that the contribution of the hard component in both systems can be represented by a $kT_{\text{br}} = 20$ keV thermal bremsstrahlung model. The galactic column densities used below were obtained from Dickey and Lockman (1990) as implemented in the EXSAS software package.

For 2022–39 we fixed the column density to the galactic value $N_{\text{H}} = 4.13 \cdot 10^{20} \text{ cm}^{-2}$ and find that the temperature range for kT_{bb} is 20–51 eV. The fluxes for both components can be taken from fits (a) and (b) in Tab. 4. Using the fluxes obtained in fit (a) with $kT_{\text{bb}} = 25$ eV we get the following ratio of bremsstrahlung vs. blackbody fluxes in the ROSAT band, $F_{\text{br}}/F_{\text{bb}} \sim 0.0003$.

For fits (c) and (e) to the 0132–65 data we used $N_{\text{H}} = 1.9 \cdot 10^{20} \text{ cm}^{-2}$ obtained in fit (d) which is about 2/3 of the galactic $N_{\text{H}} = 2.63 \cdot 10^{20} \text{ cm}^{-2}$ as these are less well constrained than fit (d). $N_{\text{H}} = 1.9 \cdot 10^{20} \text{ cm}^{-2}$ leads to a 2- σ temperature range $kT_{\text{bb}} = 15$ –48 eV for the blackbody component of 0132–65. Even though the system was a factor ~ 5 brighter during the RASS than during the pointed observations. The flux ratio $F_{\text{br}}/F_{\text{bb}} \sim 0.021$ remains almost the same. Both low values of $F_{\text{br}}/F_{\text{bb}}$ fit nicely into the picture presented by Beuermann (1997) in which the bremsstrahlung component is gradually suppressed as the magnetic field strength increases.

4. Discussion and conclusions

Our optical and X-ray observations of the soft X-ray sources 2022–39 and 0132–65 revealed that both objects are AM Her systems with comparable high magnetic field strengths (~ 67 MG and ~ 68 MG, respectively). Both systems have orbital periods of only ~ 78 min. In the case of 2022–39, it is well documented by the radial velocity curve of the Balmer and He II emission lines that the photometric period is indeed the orbital period. In 0132–65, the orbital period could in principle be twice the photometric period, but we consider this unlikely as the shape of the optical lightcurve repeats very well with the 78 min period and there is no indication that the system might show two photometric maxima per orbit.

We can confine the accretion geometry of 2022–39 as follows: The dip at phase $\varphi = 0.0$ seen in the optical, and probably also in the X-ray lightcurve is a feature which is similarly present in the lightcurves of other polars, e.g. EF Eri and EK UMa (Beuermann et al. 1987, Beuermann & Thomas 1993). It is probably caused when the accretion stream crosses our line-of-sight and occults part of the accretion region on the white dwarf. This implies that the orbital inclination i must be larger than the co-latitude δ of the accretion spot ($i > \delta$). This picture is supported by the phasing of the radial velocity curve of

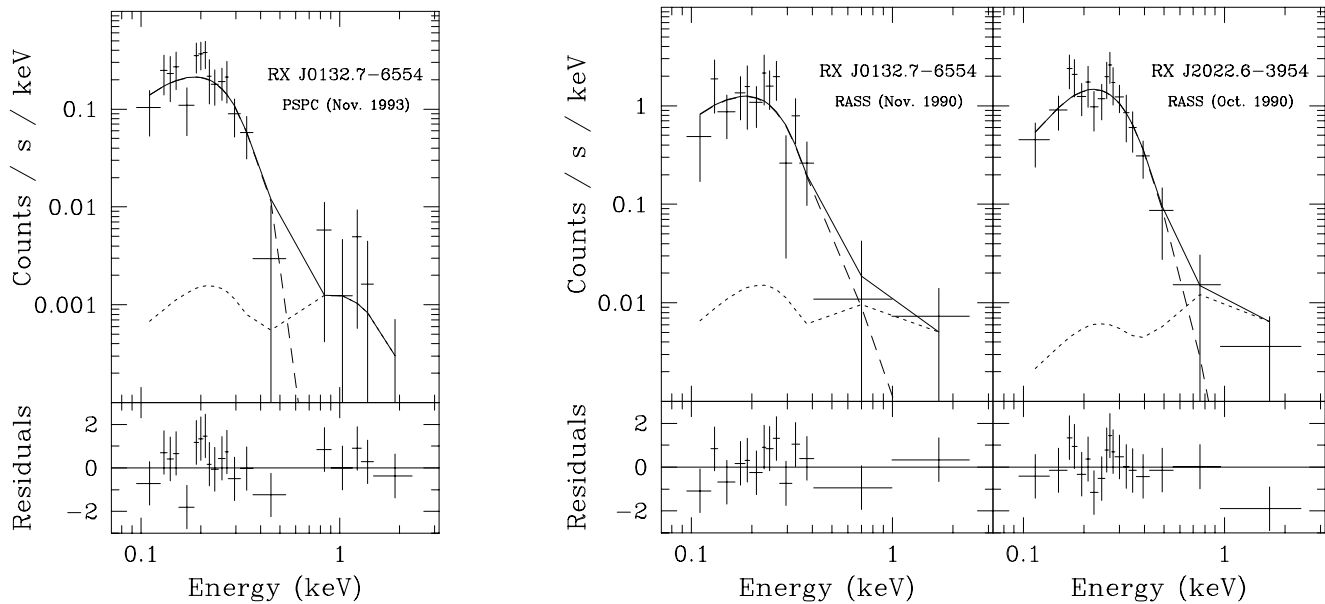


Fig. 8. X-ray spectra of 0132–65 and 2022–39 obtained with ROSAT. From left to right pointed PSPC data of 0132–65, RASS data of 0132–65, and RASS data of 2022–39. The corresponding fit parameters are given in Tab. 4 (fits (d), (c), and (a), respectively)

the emission lines which reach maximum redshift at $\varphi \sim 0.12$. As we do not resolve the broad and narrow line components which are frequently seen in higher-resolved spectra of polars, our Doppler-shift measurements certainly do not only include the magnetically confined part of the stream but also the free-falling trajectory leaving the secondary, and the narrow emission line from the heated face of the secondary. Maximum redshift, therefore, expectedly occurs shortly after the dip. During the optical maxima at phases $\varphi \sim 0.9$ and $\varphi \sim 0.25$ the cyclotron harmonics are most pronounced which is expected as the cyclotron emission is beamed orthogonally to the field lines and thus best visible when we view it perpendicular to the field lines in the accretion region. Except for the dip phase, X-ray emission is observed at all orbital phases with enhanced flux occurring between $\varphi \sim 0.6$ and $\varphi \sim 0.3$. This implies that the accretion region does not completely disappear behind the horizon during the rotation of the white dwarf and gives the constraint $i + \delta \lesssim 90^\circ$. As there is no eclipse seen of the white dwarf by the secondary star, we conclude that $45^\circ < i < 85^\circ$ and $45^\circ > \delta > 5^\circ$ for 2022–39.

A similar picture emerges from our observations of 0132–65. The large-amplitude variation of the optical flux is probably due to cyclotron beaming. This is supported by the average bright-phase and faint-phase optical spectra which show cyclotron harmonics only in the bright phase. This means that the accretion region is oriented towards the observer at $\varphi \sim 0.0$ (i.e. optical minimum) and is located at the rim of the white dwarf at $\varphi \sim 0.5$ (i.e. optical maximum). Consequently, the maximum of the soft X-ray flux occurs during the optical faint phase. The X-ray flux vanishes for ~ 0.1 of the orbit just around the optical maximum ($\varphi \sim 0.45$) which may be due to self-eclipse by the white dwarf. There may also be an X-ray dip at

$\varphi \sim 0.95$, shortly before the X-ray maximum. Like in 2022–39, this could be caused by the accretion stream crossing our line-of-sight.

0132–65 and 2022–39 have the shortest two orbital periods found so far in polars. Together with EV UMa (= RE 1307+535, Osborne et al. 1994, Hakala et al. 1994), RX J1015.5+0904 (Burwitz et al. 1996), and FH UMa (=RX J1047.1+6335, Singh et al. 1995) they form a new group of systems with orbital periods below 80 min. Prior to the ROSAT soft X-ray and the WFC EUV surveys, EF Eri ($P_{\text{orb}} \sim 81$ min has been the only system at the short-end of the period distribution (Ritter & Kolb 1992). The existence of a peak of systems with $P_{\text{orb}} \lesssim 80$ min has been predicted by evolutionary scenarios (e.g. Kolb & de Kool 1993).

At $P = 78$ min, the two new magnetic CVs are found at or close to the theoretical minimum orbital period where the companion star moves more or less rapidly towards degeneracy (Paczynski & Sienkiewicz 1981, Rappaport et al. 1982, Nelson et al. 1985, and references therein). Depending on the opacity in its atmosphere, the temperature may drop substantially, and the star becomes practically invisible. Our assumptions on its spectral type and the resulting distance estimate should be considered with caution, therefore. The long-term mass transfer rate, on the other hand stays at $\sim 10^{-11} M_{\odot}/\text{yr}$ for some time after the minimum period is passed and the system should remain a moderately luminous X-ray source. If the observed fluxes are not substantially below any long-term mean values, the expected luminosity places the systems at distances comparable to those estimated above, i.e. a few hundred parsecs.

Finally, we comment on the fact that the field strengths of the two new polars are among the largest reported so far for members of their class (see e.g. Beuermann 1997). Most po-

lars seem to crowd at field strengths below approximately 70 MG independent of orbital period (with the exception of AR UMa which has 230 MG, Schmidt et al. 1996). Contrary to neutron stars (Romani 1990), accretion seems to be ineffective in reducing the polar field strengths of white dwarfs, a situation which can be understood as a consequence of differences in the two dominant time scales, the flow time scale which carries the field into the interior of the star along with the accreted matter and the Rayleigh-Taylor time scale (among others) which tends to reestablish the field structure. In neutron stars the flow into the star is rapid and causes a secular reduction in surface field strength while in white dwarfs the flow is comparatively slow and such reduction is prevented (see Beuermann 1997).

Acknowledgements. We thank the staff at La Silla for their competent assistance during our optical observing runs and the ROSAT team for its enduring work which resulted in the All-Sky-Survey data base. We also thank the referee Dr. Martine Mouchet for her constructive comments. This work was supported by the DARA under grant 50 OR 9210,

References

- Bailey, J., 1981, MNRAS, 197, 31
- Beuermann, K., 1997, Perspectives of high-energy astronomy & astrophysics, Agrawal, P. (ed.), Tata Inst. of Fund. Res., in press
- Beuermann, K., Burwitz, V., 1995, ASP Conf. Ser. 85, 99
- Beuermann, K., Burwitz, V., Reinsch, K., Schwöpe, A.D., Thomas, H.-C., 1995, Cataclysmic Variables, Bianchini, A., Dellavalle, M., Orio, M. (eds.), Kluwer, p. 381
- Beuermann, K., Thomas, H.-C., 1993, Adv. Space Res. 13(12), 115
- Beuermann, K., Thomas, H.-C., Giommi, P., Tagliaferri, G., 1987, AA 175, L9
- Burwitz, V., Reinsch, K., Schwöpe, A.D., et al., 1996, Cataclysmic Variables and Related Objects, Evans, A., Drew, J.H. (eds.), Kluwer, p. 229
- Dickey, J.M., Lockman, F.J., 1990, ARA&A 28, 215
- Hakala, P. J., Pirola, V., Vilhu, O., Osborne, J. P., Hannikainen, D. C., 1994, MNRAS, 271, L41
- Hamuy, M., Walker, A.R., Suntzeff, N.B., 1992, PASP 104, 533
- Hamuy, M., Suntzeff, N.B., Heathcote, S.R., 1994, PASP 106, 566
- Kolb, U., de Kool, M., 1993, A&A 279, L5
- Landolt, A.U., 1992, AJ 104, 340
- Nelson, L. A., Chau, W. Y., Rosenblum, A., 1985, ApJ 299, 658
- Osborne, J. P., Beardmore, A. P., Wheatley, P. J., et al., 1994, MNRAS 270, 650
- Paczynski, B., Sienkiewicz, R., 1981, APJ 248, L101
- Ramseyer, T.F., 1994, ApJ 425, 243
- Rappaport, S., Joss, P.C., Webbink, R.F., 1982, ApJ 254, 616
- Reid, N., Gilmore, G. 1984, MNRAS 206, 19
- Ritter, H., Kolb, U., 1992, A&A 259, 159
- Romani, R.W., 1990, Nat 347, 741
- Schwöpe, A.D., 1995, Rev. Modern Astron. 8, 125
- Schmidt, G.D., Szkody, P., Smith, P.S., et al., 1996, ApJ 473, 483
- Singh, K.P., Szkody, P., Barrett, P., et al., 1995, ApJ. 453, 95
- Warner, B., 1995, Cataclysmic Variable Stars, Cambridge University Press
- Zimmermann, H.U., Belloni, T., Izzo, C., Kahabka, P., Schwentker, O., 1993, MPE Report 244

This article was processed by the author using Springer-Verlag L^AT_EX A&A style file L-AA version 3.